Purification and Biochemical Characterization of a Pyruvate-Specific Class II Aldolase, HpaI[†]

Weijun Wang[‡,§] and Stephen Y. K. Seah*[,‡]

Department of Molecular and Cellular Biology, University of Guelph, Guelph, Ontario, Canada, and College of Life Science, South China Agricultural University, Guangzhou, China

ABSTRACT: HpaI, a class II pyruvate-specific aldolase involved in the catabolic pathway of hydroxyphenylacetate, is overexpressed and purified. A previous suggestion that phosphate is involved in proton transfer of pyruvate, based on the crystal structure of the homologous 2-dehydro-3-deoxygalactarate aldolase, is not substantiated from biochemical studies with HpaI. Thus, specific activities of the enzyme for the substrate 4-hydroxy-2-ketopentanoate in sodium HEPES and Tris-acetate buffers are higher than in sodium phosphate buffer. The enzyme also catalyzed the partial reaction of pyruvate proton exchange with an initial rate of 0.77 mmol min^{-1} mg^{-1} in phosphate-free buffer, as monitored by nuclear magnetic resonance. Steady-state kinetic analysis shows that the enzyme is also able to catalyze the aldol cleavage of 4-hydroxy-2-ketohexanoate and 3-deoxy-D-*manno*-oct-2-ulosonic acid (KDO). The enzyme exhibits significant oxaloacetate decarboxylase activity, with a k_{cat} value 2.4-fold higher than the corresponding value for the aldol cleavage of 4-hydroxy-2-ketopentanoate. Sodium oxalate, an analogue of the enolate intermediate of the enzyme-catalyzed reaction, is a competitive inhibitor of the enzyme, with a K_i value of 5.5 μM. Replacement of an active site arginine residue (R70) with alanine by site-specific mutagenesis resulted in an enzyme that lacks both aldolase and decarboxylase activities. The mutant enzyme is also unable to catalyze pyruvate proton exchange. The dissociation constant for pyruvate in the R70A mutant, determined by fluorescence titration, is similar to that of the wild-type enzyme, indicating that pyruvate binding is not affected by this mutation. Together, the results show that R70 influences catalysis in HpaI, particularly at the pyruvate proton exchange step.

Aldolases catalyze reversible stereospecific C−C bond formation and are therefore useful for the chemical synthesis of enantiomerically pure pharmaceuticals, including carbohydrates and antibiotics (*1*). Diversity exists among aldolases in terms of their catalytic mechanisms and specificity for the carbonyl donor in the aldol condensation reaction. Thus, class I aldolases utilize a lysine residue which forms a Schiff base with the substrate during the reaction (*2*, *3*), while class II enzymes contain a divalent cation which stabilizes the carbanion intermediate (*4*). Class II enzymes can be further divided into subgroups depending on the nature of the carbonyl donor (*5*). The dihydroxyacetone phosphate-specific enzymes are the best characterized subgroup of class II aldolases whose members include fructose-1,6-bisphosphate, L-fuculose-1-phosphate, and L-rhamnulose-1-phosphate aldolases. These aldolases typically utilize a tetrahedral coordinated Zn^{2+} ion as a cofactor (*6*−*8*). In contrast, class II aldolases that utilize pyruvate as a carbonyl donor contain an octahedral coordinated divalent metal ion, which is usually Mg^{2+} or Mn^{2+} (*9*, *10*). There are few studies on this subgroup of enzymes despite their potential utility for the synthesis of nonphosphorylated compounds, such as derivatives of KDO[1] which are potentially useful as new antibiotics that target bacterial outer membrane lipopolysaccharide biosynthesis (*1*).

The mechanism for class II aldolases in the aldol cleavage direction involves the participation of a base which abstracts a proton from the C4 hydroxyl group of the substrate, leading to cleavage of the bond between C3 and C4 (Scheme 1). The carbanion thus formed is stabilized by the metal cofactor, and subsequent proton donation by an acid completes the reaction (*3*). Dihydroxyacetone phosphate-specific class II aldolases utilize glutamate or aspartate residues in this acid−base catalytic reaction (*7*, *8*, *11*, *12*). Catalytic residues in pyruvate-specific class II aldolases are not yet biochemically defined, although three-dimensional crystal structure analysis has provided some insight into which residues could function in catalysis. In 2-dehydro-3-deoxygalactarate (DDG)

---

* To whom correspondence should be addressed: Department of Molecular and Cellular Biology, University of Guelph, Guelph, Ontario, Canada N1G 5E9. E-mail: sseah@uoguelph.ca. Phone: (519) 824-4120, ext. 56750. Fax: (519) 837-1802.
[‡] University of Guelph.
[§] South China Agricultural University.

[1] Abbreviations: ADH, alcohol dehydrogenase; DDG, 2-dehydro-3-deoxygalactarate; HEPES, 4-(2-hydroxyethyl)-1-piperazinepropanesulfonic acid; IPTG, isopropyl β-D-thiogalactopyranoside; KDO, 3-deoxy-D-*manno*-oct-2-ulosonic acid; LDH, L-lactate dehydrogenase; MOPS, 3-(*N*-morpholino)propanesulfonic acid; NMR, nuclear magnetic resonance.

Scheme 1: Catalytic Mechanism of Class II Aldolase[a]
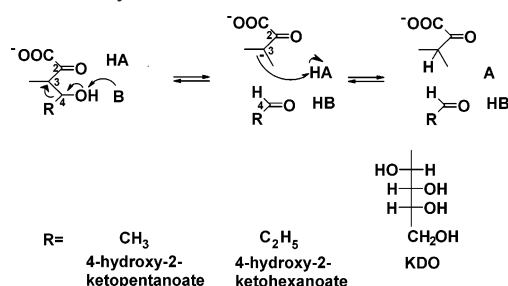
[a] The structures and names of potential substrates for pyruvate-specific aldolases are shown. Dihydroxyacetone phosphate-specific aldolases utilize substrates with a hydroxyl substituent at C3 and a methyl phosphate rather than a carboxyl substituent at C2. General acid and base catalytic residues are represented as AH and B, respectively.

aldolase, an unusual but interesting hypothesis has been proposed that involves an enzyme-bound phosphate molecule that serves to abstract or donate protons to pyruvate or enolpyruvate, respectively, during the reaction (9). This is based on the presence of phosphate anions within the active site of the substrate-free enzyme and the absence of the usual amino acids (histidine, aspartate, glutamate, and lysine) that can serve as a base in the proximity of the pyruvate methyl carbon. However, these phosphate anions are absent in the structure of the enzyme–pyruvate complex, and biochemical characterization by Fish (13) shows that the aldol cleavage activity of DDG aldolase in Tris-maleate buffer is 95% of the activity obtained with phosphate buffer (9, 13). This ambiguity in the proposed catalytic role of phosphate has not been further investigated.

Homologues of DDG aldolase can be found in the bacterial degradation pathway of some aromatic compounds, such as 3-hydroxyphenylacetate and 4-hydroxyphenylacetate (14) and the environmental pollutant tetralin (15). For example, the sequence of the aldolase HpaI in the former pathway in *Escherichia coli* W is 44% identical and 61% similar to that of DDG aldolase. Residues in DDG aldolase involved in direct or water-mediated metal ion binding (D179, E153, E49, and H50) and those that formed van der Waals contacts with pyruvate (G176 and L216) were conserved in HpaI. The substrates for DDG aldolase, HpaI, and the aldolase in the tetralin degradation pathway, ThnF, are similar as they are 4-substituted derivatives of 4-hydroxy-2-ketobutanoate, and they act on the enantiomers with an (S) configuration at C4 (16, 17). We have previously purified a number of enzymes from the meta-cleavage aromatic degradation pathway (18, 19) and are therefore able to generate enzymatically substrates for HpaI from catechols. This allows us to perform a detailed biochemical study of this enzyme and investigate the inferred phosphate requirement. Interestingly, HpaI was also found to possess significant oxaloacetate decarboxylase activity. By site-specific mutagenesis, together with spectroscopic and kinetic analysis, we report the identification of an amino acid residue that is important for pyruvate methyl proton exchange in the enzyme.

MATERIALS AND METHODS

Chemicals. Catechol, 4-methylcatechol, oxaloacetic acid, KDO ammonium salt, sodium pyruvate, sodium oxalate, L-lactate dehydrogenase (rabbit muscle), alcohol dehydrogenase (*Saccharomyces cerevisiae*), and Chelex 100 were from Sigma-Aldrich (Oakville, ON). Restriction enzymes, T4 DNA ligase, and Pfx polymerase were from Invitrogen (Burlington, ON) or New England Biolabs (Pickering, ON). All other chemicals were analytical grade and were obtained from Sigma-Aldrich and Fisher Scientific (Nepean, ON).

DNA Manipulation. DNA was purified, digested, and ligated using standard protocols (20). The *hpaI* gene was amplified by PCR using the primers with GGCACATATG-GAAAACAGTTTTAAAGC and GTCTCTGCAGTTAATA-CACGCCGGGCTTCACG sequences. Introduced NdeI and PstI restriction sites are underlined. The amplified fragment is ligated to vector pT7-7 (21). The *hpaI* gene from a positive clone was sequenced at the Guelph Molecular Supercentre, University of Guelph, to ensure there were no PCR-induced errors. Site-directed mutagenesis to create the R70A mutant of HpaI was carried out according to the QuikChange (Stratagene) method using the mutagenic oligonucleotides GCCAGCCGGTGGTAGCTCCGTCGTGGAACG and CGT-TCCACGACGGAGCTACCACCGGCTGGC (the underlined nucleotides correspond to a change from the arginine CGT codon to an alanine codon). Mutants were screened by direct DNA sequencing.

Purification of Wild-Type HpaI and Its R70A Mutant. Recombinant *E. coli* Bl21(λDE3) harboring the wild-type or mutant *hpaI* were propagated in 1 L of Luria-Bertani medium supplemented with 1.0 M D-sorbitol, 2.5 mM glycine betaine, and 100 μg/mL ampicillin at 37 °C until a density of 0.6 was reached at 600 nm. The culture was incubated on ice for 30 min, after which 0.5 mM IPTG was added to induce protein expression. The culture was incubated overnight at 18 °C with shaking and then harvested by centrifugation at 5000g for 10 min.

Chromatography was performed on an ÄKTA Explorer 100 apparatus (Amersham Pharmacia Biotech, Baie d'Urfé, PQ). Buffers containing 20 mM sodium HEPES (pH 7.5) were used throughout the purification procedure unless indicated otherwise.

The cell pellet (approximately 4 g wet weight) was resuspended in buffer containing protease inhibitors (Complete Mini, Roche Applied Science, Laval, PQ) and disrupted by being passed through a French press three times at an operating pressure of 12 000 psi. The cell debris was removed by centrifugation at 17500g for 10 min. The clear supernatant was filtered through a 0.45 μm filter and was loaded onto a Source 15Q (Amersham Pharmacia Biotech) anion exchange column (2 cm × 13 cm), which had been equilibrated with buffer. The column was washed with 2 column volumes of the buffer containing 0.1 M NaCl and then with a linear gradient of NaCl from 0.1 to 0.45 M over 12 column volumes. Fractions containing HpaI activity were eluted at ~0.3 M NaCl. Active fractions were pooled and concentrated by ultrafiltration with a YM10 filter (Millipore, Nepean, ON) and was loaded onto a phenyl-Sepharose hydrophobic interaction chromatography column (1 cm × 18.5 cm), which was pre-equilibrated with buffer containing 0.4 M ammonium sulfate. The column was washed with 2 column volumes of the same buffer and then with a 5 column volume linear gradient of ammonium sulfate from 0.4 to 0 M followed by 2 column volumes of ammonium sulfate-free buffer. Fractions containing HpaI activity were eluted at ~0.15 M ammonium sulfate. Active fractions were pooled and concentrated to ~4 mL by ultrafiltration with a YM10 filter and

then loaded onto a HiLoad 26/60 Superdex 200 prep gel filtration column (Amersham Pharmacia Biotech) that had been preequilibrated with buffer containing 0.15 M NaCl. The column was eluted with the same buffer at a flow rate of 1.0 mL/min. Fractions containing HpaI activity were pooled and concentrated as described above. The enzyme was aliquoted and stored at $-20\ ^{\circ}C$ in 20 mM sodium HEPES buffer (pH 7.5). The enzyme remained stable for 2 months under this storage condition.

Determination of Protein Concentration, Purity, and Molecular Mass. Protein concentrations were determined by the Bradford assay (*22*) using bovine serum albumin as the standard. SDS−PAGE was performed, and the gels were stained with Coomassie Blue according to established procedures (*23*). The BenchMark Protein Ladder (Invitrogen) containing proteins ranging from 10 to 220 kDa was used for the molecular mass markers.

Preparation of 4-Hydroxy-2-ketopentanoate and 4-Hydroxy-2-ketohexanoate. Catechol dioxygenase (XylE), 2-hydroxy-6-oxohepta-2,4-dienoate hydrolase (TodF), and 2-hydroxypenta-2,4-dienoate hydratase (BphH) were purified according to previously reported procedures (*19*).

4-Hydroxy-2-ketopentanoate and 4-hydroxy-2-ketohexanoate were generated enzymatically from catechol and 4-methylcatechol, respectively, using a modification of a published protocol (*24*). Briefly, 6.0 mM catechol, 200 μg of XylE, 1 mg of TodF, and 100 μg of BphH in 20 mM sodium HEPES (pH 7.5) (200 mL) were stirred over the course of 12 h at room temperature. Then, 1 g of activated carbon was added and the mixture centrifuged at 17500g for 10 min to remove unreacted catechols. The supernatant was acidified with concentrated HCl to a final concentration of 2.0 M, and the mixture was centrifuged at 17500g for 10 min to remove the precipitated protein. The supernatant was then incubated at 100 $^{\circ}$C for 15 min to allow 4-hydroxy-2-ketopentanoate or 4-hydroxy-2-ketohexanoate to convert to 2-keto-4-methyl-γ-butyrolactone or 2-keto-4-ethyl-γ-butyrolactone which can be extracted into ethyl acetate. The ethyl acetate fraction was evaporated to dryness using a vacuum. The white solid (lactone) was hydrolyzed at room temperature for 12 h in a pH 8.5 solution to obtain 4-hydroxy-2-ketopentanoate or 4-hydroxy-2-ketohexanoate. The concentrations of the respective substrates were determined by coupling their aldol cleavage by excess HpaI with L-lactate dehydrogenase (LDH). The total amounts of pyruvate produced are calculated from the spectrophotometrically determined stoichiometric oxidation of NADH by LDH. Pure sodium pyruvate was used as a standard.

Enzyme Assays. All kinetics assays were performed at least in duplicate at 25 $^{\circ}$C using a Varian Cary 3 spectrophotometer equipped with a thermojacketed cuvette holder. HpaI activity was deduced by determining the rate of pyruvate formation by coupling with NADH oxidation using LDH at 340 nm. The extinction coefficient of NADH was taken to be 6200 $M^{-1}\ cm^{-1}$; 1.0 unit of enzyme represents the amount of protein that produces 1 μmol of pyruvate from substrate in 1 min.

Routine assays of HpaI activity during protein purification contained 1.5 mM 4-hydroxy-2-ketopentanoic acid, 0.5 mM CoCl$_2$, 0.3 mM NADH, and 30 units of LDH in a total of 1 mL of 100 mM sodium HEPES (pH 8.0). The assay reaction was initiated by the addition of HpaI.

Assays for determining the substrate specificity of enzymes were carried out under similar conditions except that the substrate concentrations were varied from at least $0.1K_m$ to $5K_m$. Oxaloacetate decarboxylase activity was determined using the same coupled assay. The background decarboxylation rate determined without the addition of HpaI was subtracted from the assay containing HpaI to obtain the enzyme-catalyzed rate. Acetoacetate decarboxylase activity was assayed by the method of Fridovich (*25*) by monitoring the decrease in absorbance at 270 nm. The final assay volume of 1.0 mL contained 5 mM acetoacetate, 0.5 mM CoCl$_2$, and 100 mM sodium HEPES (pH 8.0). The extinction coefficients of acetoacetate and acetone are 55.0 and 28.3 $M^{-1}\ cm^{-1}$, respectively. Data were fitted by nonlinear regression to the Michelis−Menten equation (for KDO) and substrate inhibition equation (all other substrates) using Leonora (*26*).

For inhibition assays, concentrations of pyruvate and sodium oxalate were varied from $0.5K_i$ to $10K_i$. In the pyruvate inhibition assay, 30 units of alcohol dehydrogenase was used instead of LDH, to couple the formation of the acetaldehyde product to NADH oxidation. Data for both the pyruvate and oxalate inhibition assays were fitted to a competitive inhibition equation using Leonora (*26*).

To ascertain if phosphate is required for HpaI activity, the specific activity of the enzyme toward 4-hydroxy-2-ketopentanoate was determined using 100 mM sodium HEPES, Tris-HCl, Tris-acetate, and sodium phosphate buffers (pH 8.0). Concentrations of assay components are the same as the standard assay.

Determination of Metal Ion Cofactor Specificity. A metal ion cofactor-free apo-HpaI solution was prepared by adding 0.5 g of Chelex 100 (Sigma) to 10 mg of purified HpaI in 10 mL of 20 mM sodium HEPES (pH 7.5). After the mixture had been stirred for 30 min, Chelex 100 was removed by centrifugation at 17500g for 10 min. The clear supernatant was apo-HpaI, which has less than 0.1% of activity compared to the activity in the presence of 0.5 mM CoCl$_2$.

Assays for determining the specific activity of the purified apoenzyme with different metal ions contained 0.15 μg of enzyme, 1.5 mM 4-hydroxy-2-pentanoate, the respective metal chloride salts (0.5 mM), 0.3 mM NADH, and 30 units of LDH in 100 mM sodium HEPES buffer (pH 8.0). Since Zn^{2+} significantly inhibits the activity of LDH, a discontinuous assay was employed. The 1.0 mL assay solution contained 1.5 mM 4-hydroxy-2-ketopentanoate, 0.5 mM ZnCl$_2$, and 0.03 μg of HpaI. The reaction mixture was incubated at 25 $^{\circ}$C for 2, 5, and 10 min, and then terminated by the addition of 5.0 mM Na$_2\cdot$EDTA. The concentration of pyruvate formed at each time point is determined by coupling it to the stoichiometric oxidation of NADH by LDH.

The apparent K_m values for Co^{2+}, Mg^{2+}, and Mn^{2+} were determined by the kinetic analysis of divalent metal ion-dependent 4-hydroxy-2-pentanoate aldolase reactions catalyzed by HpaI. The enzyme was incubated and assayed with the respective divalent metal chloride salts at concentrations varying from at least $0.1K_{m(app)}$ to $20K_{m(app)}$. The concentration of 4-hydroxy-2-ketopentanoate was fixed at 1.5 mM. All other conditions were the same as those of the standard activity assay. Apparent K_m values [$K_{m(app)}$] were calculated

by fitting the data to the following equation by nonlinear regression in Leonora.

$$v = \frac{V_{max}[M]}{K_{m(app)} + [M]}$$

where v is the initial velocity at various concentrations of metal ions and V_{max} is the maximal catalytic rate at saturating metal ion concentration.

Protein Fluorescence Measurements. Fluorescence spectra were recorded using the Eclipse fluorescence spectrometer (Varian). Samples contain 90 μg/mL HpaI in 1.0 mL of 100 mM sodium HEPES buffer (pH 8.0). Pyruvate, CoCl$_2$, and acetaldehyde were added at final concentrations of 2.0, 0.5, and 2.0 mM, respectively. Samples were excited at 295 nm, and the emission spectra were scanned from a wavelength of 300 to 450 nm. The peak intensities of the spectra at a wavelength of 335 nm were recorded.

Equilibrium dissociation constants of pyruvate in the wild-type and R70A enzymes were determined by titration. Samples were excited at 295 nm, and the emission fluorescence were detected at 335 nm. The concentration of enzymes in all measurements was fixed at 90 μg/mL, and the protein emission fluorescence was recorded in the presence of varying concentrations of pyruvate in 0.1 mL of 100 mM sodium HEPES (pH 8.0). The dissociation constant (K_d) can be determined by fitting the data to the following equation by nonlinear regression using Leonora (*26*).

$$\Delta F = \frac{\Delta F_{max} + [L]}{K_d + [L]}, \Delta F = F_0 - F$$

where F is the protein fluorescence intensity at varying concentrations of pyruvate [L] and F_0 is the fluorescence intensity of the protein in the absence of pyruvate.

Proton Exchange of Pyruvate Catalyzed by Wild-Type and Mutant HpaI. The rate of pyruvate proton exchange was determined by measuring the loss of the pyruvate methyl proton signal in deuterated buffer by NMR, following a previously reported protocol (*27*). To obtain enzyme samples in deuterated MOPS buffer (pD 8.0), 300 μg of wild-type and R70A enzyme were concentrated by filtration over a Microcon-30 concentrator (Millipore) from a volume of 300 to 30 μL. Deuterated buffer was then added to the concentrated protein to a final volume of 300 μL. This procedure was repeated three times.

The proton exchange reactions were performed with a Bruker Avance 600 MHz spectrometer at 25 °C using a 5.0 mm NMR tube with an assay solution of 600 μL containing 30 mM pyruvate, 0.5 mM CoCl$_2$, 5.25 μg of HpaI, and 20 mM deuterated MOPS buffer (pD 8.0). After the enzyme was added to the reaction mixture, the ^{1}H NMR spectra of samples were recorded every 3 min over a period of 30 min. HpaI, inactivated by heat denaturation at 100 °C for 10 min, and sample without enzyme serve as the negative controls. Proton exchange was assessed from the time-dependent change in the ratio of the methyl proton signal of pyruvate (2.38 ppm) to the reference methylene protons at position 1 of MOPS (2.05 ppm), which is unaffected by the exchange
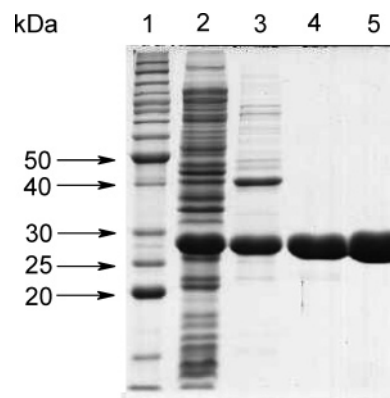

FIGURE 1: Coomassie Blue-stained SDS−PAGE of purified HpaI. The gel was loaded with samples of HpaI from crude extract (lane 2), a preparation after anion exchange (lane 3), a preparation after hydrophobic column chromatography (lane 4), and a preparation after gel filtration (lane 5). The molecular masses of the proteins in the standard (lane 1) are indicated beside the gel. The molecular mass of HpaI monomers as determined from the gel is 28.0 kDa.

reaction. The observable proton exchange constant (k_{obs}) is determined using the equation

$$k_{obs} = k_{enzyme} - k_{control}$$

where k_{enzyme} and $k_{control}$ are constants derived from data with and without the enzyme, respectively. These constants are the negative slopes of the least-squares fit of the data plotted as the natural log of peak ratios of pyruvate and MOPS versus time.

The initial proton exchange rate ($V_{exchange}$) can be determined by the following equation (*28*):

$$V_{exchange} = \frac{3k_{obs}[pyruvate]}{[enzyme]}$$

where [pyruvate] is the concentration of pyruvate in the assay solution (in terms of millimoles per liter) and [enzyme] is the concentration of HpaI in the assay solution (in terms of milligrams per liter).

RESULTS

Expression and Purification of HpaI. HpaI is expressed in *E. coli* BL21(λDE3) under the control of the T7 promoter from expression plasmid pT7-7. Lowering the growth temperature to 18 °C together with the addition of sorbital and the compatible solute, glycine betaine, to the media significantly improved the expression of soluble HpaI. These same conditions have been reported to enhance the solubility and proper folding of other recombinant proteins expressed in *E. coli* (*29, 30*). Soluble HpaI is purified to homogeneity using anion exchange, hydrophobic interaction, and gel filtration chormatography with a typical yield of 11 mg of purified protein per liter of bacterial culture (Figure 1 and Table 1). The subunit molecular mass of the enzyme as estimated by SDS−PAGE is 28.0 kDa, which is in agreement with the predicted molecular mass calculated from the amino acid sequence.

Metal Ion Specificity. The specific activities of purified apo-HpaI with different metal ions were determined (Table 2). The highest specific activities, with 4-hydroxy-2-keto-pentanoate as the substrate, were obtained with Co^{2+} and

Table 1: Purification of HpaI[a]

purification step	total protein (mg)	total activity (units)	specific activity (units/mg of protein)	purification (n-fold)	recovery (%)
crude extract	234.6	1.0×10^4	42.6	1.0	100
Source Q15	35.2	8.2×10^3	233.0	5.5	81.9
Phenyl-Sepharose	19.3	5.7×10^3	295.3	6.9	56.5
Superdex200	11.2	3.8×10^3	339.3	8.0	38.1

[a] HpaI was purified from 1 L of cells. Assays contain 1.5 mM 4-hydroxy-2-ketopentanoate, 0.5 mM $CoCl_2$, 0.3 mM NADH, and 30 units of LDH in 100 mM sodium HEPES buffer (pH 8.0). One unit is the enzyme required to produce 1 μmol of pyruvate per min.

Table 2: Relative Activities of HpaI with Various Metal Ions[a]

metal ion	relative activity (%)
Mn^{2+}	100 ± 1.22
Co^{2+}	99.36 ± 2.82
Zn^{2+}	72.94 ± 3.34
Fe^{2+}	57.15 ± 3.14
Mg^{2+}	48.90 ± 1.24
Ni^{2+}	11.47 ± 0.23
Cd^{2+}	3.89 ± 0.55
Cu^{2+}	0.73 ± 0.27

[a] Activity obtained with $MnCl_2$ is taken as 100%. Assays, with the exception of that for Zn^{2+}, were performed with 0.15 μg of HpaI, 1.5 mM 4-hydroxy-2-ketopentanoate, the respective metal chloride salt at 0.5 mM, 0.3 mM NADH, 30 units of LDH, and 100 mM sodium HEPES buffer (pH 8.0) in a total volume of 1 mL. Activity with Zn^{2+} was determined by a discontinuous method as described in Materials and Methods.

Table 3: Specific Activities of HpaI in Buffers (pH 8.0) with Different Compositions[a]

buffer	specific activity (units/mg)
sodium HEPES	324.8 ± 28.2
Tris-HCl	256.0 ± 1.4
Tris-acetate	300.9 ± 2.3
sodium phosphate	264.4 ± 1.5

[a] The assay contains 1.5 mM 4-hydroxy-2-ketopentanoate, 0.5 mM $CoCl_2$, 0.3 mM NADH, and 30 units of LDH in a final volume of 1.0 mL of the respective buffer (100 mM).

Mn^{2+} ions. Other divalent cations activate the enzyme in the following order of effectiveness: $Zn^{2+} > Fe^{2+} > Mg^{2+} > Ni^{2+} > Cd^{2+} > Cu^{2+}$. The enzyme is not active with Ca^{2+}, Fe^{3+}, Cr^{3+}, and Al^{3+}.

Apparent K_m values of HpaI toward Co^{2+}, Mg^{2+}, and Mn^{2+} were determined by steady-state kinetic analysis of the metal-dependent aldol cleavage of 4-hydroxy-2-ketopentanoate. The enzyme has the lowest $K_{m(app)}$ for Co^{2+}, with a value of 6.0 ± 0.9 μM. The corresponding values for Mn^{2+} and Mg^{2+} are 17.5 ± 1.7 and 289.3 ± 38.6 μM, respectively. Co^{2+} is used as a cofactor in subsequent analysis.

Determining the Requirement for Phosphate in Overall and Partial Reactions. To ascertain if phosphate is essential for HpaI activity, assays were performed in buffers (pH 8.0) with different chemical compositions (Table 3). The enzyme is catalytically competent in sodium HEPES, Tris-HCl, and Tris-acetate buffers. In fact, the specific activities with sodium HEPES and Tris-acetate buffers are 20 and 10% higher, respectively, compared to the activity in sodium phosphate buffer. Additions of 5 mM sodium phosphate in sodium HEPES buffer led to a 5.3% reduction in specific activity.
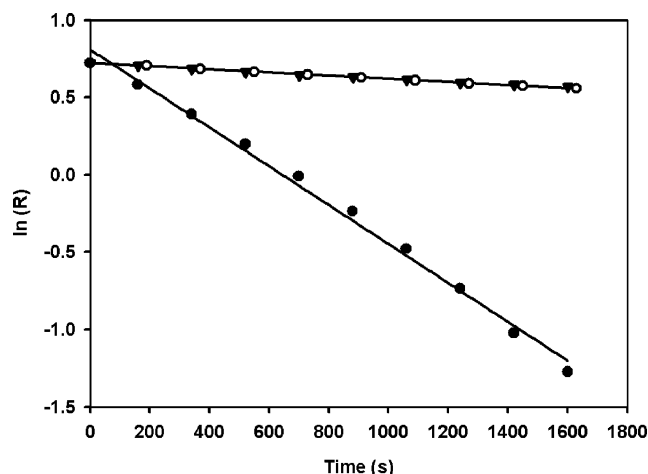

FIGURE 2: HpaI-catalyzed pyruvate methyl proton exchange in deuterated MOPS buffer. Enzyme-catalyzed exchange of pyruvate methyl protons was performed using 600 μL of assay solution containing 30 mM pyruvate, 0.5 mM $CoCl_2$, and 20 mM deuterated MOPS buffer (pD 8.0) in the absence of enzyme (▼), in the presence of 5.25 μg of HpaI (●), or in the presence of 5.25 μg of heat-inactivated HpaI (○). Data were plotted as the natural log ratio (R) of the proton signal of pyruvate and MOPS vs time.

We next examine if HpaI is able to catalyze the partial reaction of pyruvate methyl proton exchange in phosphate-free buffer (MOPS buffer). Using NMR, we monitor the reduction of the pyruvate methyl proton signal as a result of enzyme-catalyzed exchange with D_2O (Figure 2). The initial rate of proton exchange by the HpaI–Co^{2+} complex is determined to be 0.77 mmol min^{-1} mg^{-1}, whereas only the background exchange rate was observed with heat-inactivated HpaI. Together, the results indicate that phosphate is not necessary for catalysis and is not responsible for pyruvate proton exchange.

Steady-State Kinetic Analysis of HpaI. The substrate specificity of HpaI was determined by steady-state kinetics. The enzyme was found to catalyze the aldol cleavage of 4-hydroxy-2-ketopentanoate, 4-hydroxy-2-ketohexanoate, and KDO (Table 4). Kinetics with KDO as the substrate obey classic Michaelis–Menten kinetics, while those of 4-hydroxy-2-ketopentanoate and 4-hydroxy-2-ketohexanoate obey the substrate inhibition model. A plot of initial velocity versus 4-hydroxy-2-ketopentanoate concentrations is shown in Figure 3.

The enzyme has the highest specificity constant for 4-hydroxy-2-ketohexanoate, that is, one carbon longer that the next best substrate, 4-hydroxy-2-ketopentanoate. This is mainly attributed to a 2.4-fold lower K_m value for 4-hydroxy-2-ketohexanoate. The specificity constant for KDO is $\sim$37000-fold lower than that for 4-hydroxy-2-ketohexanoate, which is due to a 417-fold lower turnover number and a 90-fold higher K_m value for this substrate. Interestingly, HpaI also possesses oxaloacetate decarboxylase activity, with a k_{cat} value that is 3.8-fold higher than that of 4-hydroxy-2-ketohexanoate. Oxaloacetate has a carboxyl substituent, and the catalytic promiscuity of HpaI can be rationalized by considering the common step of carbon–carbon bond cleavage between C3 and C4, followed by proton donation of an enolate intermediate during both the aldol and decarboxylation reaction. HpaI was not able to catalyze the decarboxylation of acetoacetate.

Table 4: Steady-State Kinetic Parameters of HpaI with Different Substrates

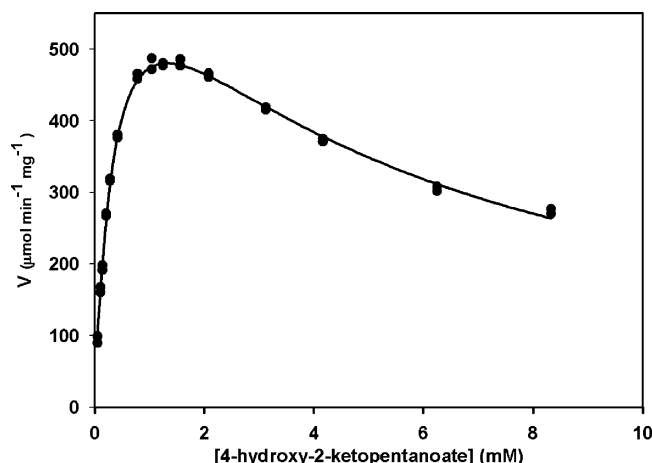| substrate	K_m (mM)	K_{si} (mM)	k_{cat} (s^{-1})	k_{cat}/K_m (M^{-1} s^{-1})
4-hydroxy-2-ketopentanoate	0.38 ± 0.01	4.56 ± 0.14	353.46 ± 5.70	9.40 × 10^5
4-hydroxy-2-ketohexanoate	0.16 ± 0.01	16.51 ± 3.75	229.36 ± 3.65	1.46 × 10^6
KDO	14.22 ± 0.22	*a*	0.55 ± 0.01	38.68
oxaloacetate (OAA)	1.37 ± 0.15	4.10 ± 0.52	866.79 ± 6.52	6.33 × 10^5

a Substrate inhibition was not observed.

FIGURE 3: Plot of the initial velocity vs the concentration of 4-hydroxy-2-ketopentanoic acid. The assay mixture contains 0.5 mM CoCl$_2$, 0.3 mM NADH, 30 units of LDH, and varying concentrations of 4-hydroxy-2-ketopentanoate in 100 mM sodium HEPES (pH 8.0). The data were fitted by nonlinear regression to the substrate inhibition equation using Leonora (*26*).

FIGURE 4: Active site structure of DDG aldolase showing the relative positions of arginine 75 (R75), the Mg^{2+} cofactor, Mg^{2+} ligands, and the bound pyruvate substrate. Mg^{2+} is represented as a cyan sphere, while the water ligands are represented as red spheres. Carbon atoms in the stick representations are colored green except in pyruvate, in which they are colored orange. Possible interactions between residues and the substrate or metal cofactor are represented by dashed lines. Coordinates for the DDG aldolase−pyruvate complex were obtained from the Protein Data Bank (entry 1DXF).

Product inhibition studies show that pyruvate is a competitive inhibitor of the 4-hydroxy-2-ketopentanoate aldolase activity with a K_i of 0.53 ± 0.03 mM. Sodium oxalate is also a competitive inhibitor of the enzyme with a K_i value of 0.0055 ± 0.0002 mM, which is 100-fold lower than the K_i of pyruvate. This compound is a structural analogue of the enolate intermediate, and its effective inhibition of enzyme activity is consistent with the formation of this intermediate in the reaction mechanism.

Role of Arginine 70 in HpaI. In the structure of DDG aldolase, the guanidino nitrogen group of arginine 75 is ∼4 Å from the pyruvate methyl carbon and 3.5 Å from the pyruvate carbonyl oxygen (Figure 4). This residue is conserved in HpaI (R70) and ThnF, the aldolase from the degradation pathway of tetralin. To determine the role of arginine 70 in HpaI, we replaced it with alanine. The R70A mutant is expressed well in *E. coli* and can be purified to homogeneity using the same protocol that was used for the wild-type enzyme. Purified R70A is, however, totally devoid of any aldolase or oxaloacetate decarboxylase activity. The mutant enzyme is also unable to catalyze proton exchange of pyruvate as determined by NMR.

Equilibrium Dissociation Constants of Pyruvate for Wild-Type and R70A Mutant Enzymes Monitored by Fluorescence Spectroscopy. To ascertain if the R70 is involved in substrate binding, we determined the dissociation constant for pyruvate using fluorescence titration. Close inspection of the three-dimensional structure of DDG aldolase reveals the presence of a single tryptophan residue (W24) within the active site of the enzyme. This residue is conserved in HpaI (W19). Tryptophan fluorescence quenching was observed with the addition of pyruvate, but not acetaldehyde, to apo-HpaI. The
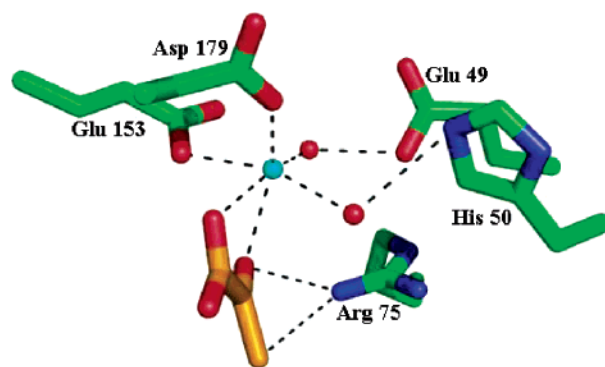
Table 5: Tryptophan Fluorescence Quenching by Pyruvate and CoCl$_2$[a]

sample	emission fluorescence intensity (units)	relative fluorescence intensity (%)
apo-HpaI	407.8	100
apo-HpaI and 2.0 mM pyruvate	371.3	91.0
apo-HpaI, 2.0 mM pyruvate, and 0.5 mM CoCl$_2$	178.9	43.9

[a] All samples contain 90 μg/mL apo-HpaI and 100 mM sodium HEPES buffer (pH 8.0) in a total volume of 1.0 mL. Samples were excited at 295 nm, and the emission fluorescence was detected at a wavelength of 335 nm. The fluorescence intensity for apo-HpaI is taken as 100%.

metal cofactor, Co^{2+}, alone does not quench the fluorescence of apo-HpaI. However, the metal ion enhances fluorescence quenching by pyruvate, indicating a further conformation change in the enzyme due to the formation of the ternary complex (Table 5). No further fluorescence quenching was observed when acetaldehyde was added to the equilibrium mixture of the enzyme, Co^{2+}, and pyruvate. Similar observations in fluorescence quenching by the various substrates were found for the R70A mutant. Fluorescence titration was then used to determine the dissociation constants for pyruvate in the wild type and R70A mutant. In both the wild-type and mutant enzymes, the presence of the metal cofactor reduced the dissociation constant of the enzyme for pyruvate by ∼60-fold (Table 6). The results also show that the affinity of the R70A mutant for pyruvate, in the presence or absence of Co^{2+}, is similar to the corresponding values for the wild-

Table 6: Equilibrium Dissociation Constants of Pyruvate for Wild-Type and R70A Mutant Enzymes[a]

enzyme	K_d for pyruvate (mM)
wild type	21.2 ± 2.4
wild type with 0.5 mM Co^{2+}	0.322 ± 0.021
R70A	26.9 ± 3.1
R70A with 0.5 mM Co^{2+}	0.467 ± 0.010

[a] The concentrations of enzymes in all measurements were fixed at 90 μg/mL, and the protein emission fluorescence was recorded in the presence of varying concentrations of pyruvate in a total of 0.1 mL of 100 mM sodium HEPES (pH 8.0).

type enzyme. Thus, R70 influences catalysis rather than substrate binding in the enzyme.

DISCUSSION

Aldolases are evolutionarily diverse enzymes that catalyze the reversible cleavage of carbon−carbon bonds. Among the class II aldolases, L-fuculose-1-phosphate and L-rhamulose-1-phosphate aldolases adopt α and β folds. They utilize a single residue (glutamate) for acid/base catalysis (*7*, *8*). Fructose-1,6-bisphosphate aldolase, on the other hand, adopts a TIM barrel fold, and its catalytic mechanism involves the participation of two catalytic residues: an aspartate that abstracts a proton at C4 of the substrate and a glutamate that donates a proton to the C3 carbanion intermediate (*11*, *12*). The pyruvate-specific aldolase, DDG aldolase, also adopts a TIM barrel fold but differs from fructose-1,6-bisphosphate aldolase in terms of the metal ion cofactor, the metal ligands, and the residues within the active site.

HpaI is homologous to DDG aldolase and was found to have the highest activity with Co^{2+} and Mn^{2+} as the cofactor. It exhibits broad substrate specificity and is able to catalyze the aldol cleavage of substrates five to eight carbon atoms long. The enzyme is able to catalyze the decarboxylation of oxaloacetate but not acetoacetate. Both the retro-aldol cleavage and oxaloacetate decarboxylation reactions lead to the formation of an enolate intermediate. This intermediate is stabilized in the enzyme by its bidentate chelation to the positively charged metal cofactor. Thus, acetoacetate, which differs from oxaloacetate in that the C1 carboxyl is replaced with a methyl group, was not decarboxylated by HpaI.

Consistent with the formation of an enolate intermediate in the aldolase reaction, HpaI is strongly inhibited by sodium oxalate. Previous structural analysis of the pyruvate-specific DDG aldolase suggests that a phosphate anion may serve as a proton donor of the enolpyruvate intermediate (*9*). Results reported here for the homologous HpaI show that the specific activities of the enzyme in phosphate-free buffers are higher by 10−20% compared to the value obtained with phosphate buffer. In addition, HpaI can catalyze methyl proton exchange of pyruvate in the absence of phosphate, as determined by NMR. Therefore, phosphate does not appear to be involved in catalysis. It should also be noted that despite the use of phosphate buffer in the crystallization of the DDG aldolase−pyruvate complex, phosphate is not present within the structure of the enzyme−substrate complex (*9*).

Inspection of the structure of the DDG aldolase−pyruvate complex shows that the guanidino nitrogen of arginine 75 (arginine 70 in HpaI) is positioned ∼4 Å from the bound pyruvate methyl carbon and 3.5 Å from the pyruvate carbonyl oxygen. Replacement of this conserved arginine

residue with alanine in HpaI led to the complete abolishment of enzyme activity. In addition, the mutant enzyme was unable to catalyze the partial reaction of pyruvate methyl proton exchange. This lack of activity is not due to impaired substrate binding, since the dissociation constants for pyruvate in the apoenzyme and Co^{2+} enzyme are comparable to the values obtained for the wild-type enzyme. Possible roles of this arginine residue include the stabilization of the negatively charged enolate intermediate or direct and water-mediated participation as a proton donor and acceptor of pyruvate and enolate, respectively. The high pK_a value (12.48) of the guanidino group of arginine seems to be incompatible with its role in proton transfer. However, in the structure of the DDG aldolase−pyruvate complex, the methyl carbon of pyruvate is in a hydrophobic environment (*9*), and the proximity of R75 in this region of the active site may result in a lowered side chain pK_a. The involvement of arginine residues in proton transfer is not without precedence, as this has been described in other enzyme systems (*31*). Alternatively, water may serve as a proton acceptor or donor, and the arginine residue may be important in positioning or activating a water molecule for proton transfer. A water ligand to a divalent metal ion has been suggested to act as a base in other enzymes, such as CMP−KDO synthetase (*32*), and indeed, one of the water ligands to the metal cofactor in DDG aldolase is 4.2 Å from the pyruvate methyl carbon. This water ligand forms a hydrogen bond with histidine 50. However, both the water ligand and imidazole nitrogen of histidine 50 are relatively distant (4.8−5 Å) from the guanidino nitrogen of arginine 75. The dissociation constant of pyruvate in Co^{2+}-bound HpaI is not affected by the replacement of arginine with alanine, thus providing additional evidence that this mutation has not perturbed the position of ligands to the metal ion cofactor. Additional experimental studies, including the construction and characterization of other mutants, are nevertheless required to determine the precise role of the arginine residue and the possible catalytic role of water ligands in the aldolase.

HpaI and DDG aldolase are related to the phospho-enolpyruvate/pyruvate superfamily of TIM barrel enzymes (*33*). Like HpaI, some members of this family of enzymes, such as phosphoenolpyruvate carboxylase, have also been reported to possess secondary oxaloacetate decarboxylase activity (*34*). The decarboxylase activity and the physiologically relevant reaction catalyzed by these enzymes appear to share a common chemical step in the formation of an enolate pyruvate intermediate. Interestingly, arginine residues, equivalent to R70 of HpaI, are present in phospho-enolpyruvate carboxylase and pyruvate phosphate dikinase, as determined by structure-based sequence alignment (*33*). Replacement of these arginine residues in *Flaveria trinervia* phosphoenolpyruvate carboxylase (R450) (*35*) and *Clostridium symbiosum* pyruvate phosphate dikinase (R617) (*36*) with glycine and lysine, respectively, led to enzymes with insignificant or no catalytic activity. The specific catalytic step that is deficient in these mutants has not been investigated in detail. Given that functionally divergent members of an enzyme superfamily usually share a common partial reaction chemistry (*37*), it is possible that the arginines in these two other enzymes serve the same function as in HpaI.

Aldolases have attracted increasing interest from the biotechnological industry because of their potential use in

the synthesis of a variety of biologically important carbohydrates. Therefore, both rational and directed evolution approaches have been used to create aldolases with desirable properties (*38*−*40*). It appears that the pyruvate-specific enzyme reported here utilizes distinct residue(s) to catalyze the enolization of the carbonyl donor as compared to the dihydroxyacetone phosphate-specific enzymes. Future work, aimed at identifying the residue(s) involved in C4−OH proton abstraction, would provide an additional point of reference for comparison with other aldolases. This may form the basis for protein engineering experiments aimed at designing aldolases with novel specificity or enhanced activity for a wider range of applications.

ACKNOWLEDGMENT

REFERENCES

1. Takayama, S., McGarvey, G. J., and Wong, C. H. (1997) Microbial aldolases and transketolases: New biocatalytic approaches to simple and complex sugars, *Annu. Rev. Microbiol. 51*, 285−310.
2. Choi, K. H., Shi, J., Hopkins, C. E., Tolan, D. R., and Allen, K. N. (2001) Snapshots of catalysis: The structure of fructose-1,6-(bis)phosphate aldolase covalently bound to the substrate dihydroxyacetone phosphate, *Biochemistry 40*, 13868−13875.
3. Horecker, B. L., Lai, C. Y., and Lai, C. Y. (1972) Aldolases, in *The Enzymes*, pp 213−258, Academic Press, New York.
4. Morse, D. E., and Horecker, B. L. (1968) The mechanism of action of aldolases, *Adv. Enzymol. Relat. Areas Mol. Biol. 31*, 125−181.
5. Drueckhammer, D. G., Hennen, W. J., Pederson, R. L., Barbas, C. F., Gautheron, C. M., Krach, T., and Wong, C. H. (1991) Enzyme Catalysis in Synthetic Carbohydrate-Chemistry, *Synthesis*, 499−525.
6. Cooper, S. J., Leonard, G. A., McSweeney, S. M., Thompson, A. W., Naismith, J. H., Qamar, S., Plater, A., Berry, A., and Hunter, W. N. (1996) The crystal structure of a class II fructose-1,6-bisphosphate aldolase shows a novel binuclear metal-binding active site embedded in a familiar fold, *Structure 4*, 1303−1315.
7. Joerger, A. C., Gosse, C., Fessner, W. D., and Schulz, G. E. (2000) Catalytic action of fuculose 1-phosphate aldolase (class II) as derived from structure-directed mutagenesis, *Biochemistry 39*, 6033−6041.
8. Kroemer, M., Merkel, I., and Schulz, G. E. (2003) Structure and catalytic mechanism of L-rhamnulose-1-phosphate aldolase, *Biochemistry 42*, 10560−10568.
9. Izard, T., and Blackwell, N. C. (2000) Crystal structures of the metal-dependent 2-dehydro-3-deoxy-galactarate aldolase suggest a novel reaction mechanism, *EMBO J. 19*, 3849−3856.
10. Manjasetty, B. A., Powlowski, J., and Vrielink, A. (2003) Crystal structure of a bifunctional aldolase-dehydrogenase: Sequestering a reactive and volatile intermediate, *Proc. Natl. Acad. Sci. U.S.A. 100*, 6992−6997.
11. Plater, A. R., Zgiby, S. M., Thomson, G. J., Qamar, S., Wharton, C. W., and Berry, A. (1999) Conserved residues in the mechanism of the *E. coli* Class II FBP-aldolase, *J. Mol. Biol. 285*, 843−855.
12. Zgiby, S., Plater, A. R., Bates, M. A., Thomson, G. J., and Berry, A. (2002) A functional role for a flexible loop containing Glu182 in the class II fructose-1,6-bisphosphate aldolase from *Escherichia coli*, *J. Mol. Biol. 315*, 131−140.
13. Fish, D. C. (1964) The metabolism of D-glucaric acid in *Escherichia coli*, Ph.D. Thesis, The University of Michigan, Ann Arbor, MI.
14. Prieto, M. A., Diaz, E., and Garcia, J. L. (1996) Molecular characterization of the 4-hydroxyphenylacetate catabolic pathway of *Escherichia coli* W: Engineering a mobile aromatic degradative cluster, *J. Bacteriol. 178*, 111−120.
15. Hernaez, M. J., Floriano, B., Rios, J. J., and Santero, E. (2002) Identification of a hydratase and a class II aldolase involved in biodegradation of the organic solvent tetralin, *Appl. Environ. Microbiol. 68*, 4841−4846.
16. Collinsworth, W. L., Chapman, P. J., and Dagley, S. (1973) Stereospecific enzymes in the degradation of aromatic compounds by *Pseudomonas putida*, *J. Bacteriol. 113*, 922−931.
17. Fish, D. C., and Blumenthal, H. J. (1966) 2-Keto-3-deoxy-D-glucarate Aldolase, *Methods Enzymol. 9*, 529−535.
18. Seah, S. Y. K., Terracina, G., Bolin, J. T., Riebel, P., Snieckus, V., and Eltis, L. D. (1998) Purification and preliminary characterization of a serine hydrolase involved in the microbial degradation of polychlorinated biphenyls, *J. Biol. Chem. 273*, 22943−22949.
19. Wang, P., and Seah, S. Y. K. (2005) Determination of the metal ion dependence and substrate specificity of a hydratase involved in the degradation pathway of biphenyl/chlorobiphenyl, *FEBS J. 272*, 966−974.
20. Sambrook, J., Fritsch, E. F., and Maniatis, T. (1989) *Molecular cloning: A laboratory manual*, Cold Spring Harbor Laboratory Press, Plainview, NY.
21. Tabor, S., and Richardson, C. C. (1985) A bacteriophage T7 RNA polymerase/promoter system for controlled exclusive expression of specific genes, *Proc. Natl. Acad. Sci. U.S.A. 82*, 1074−1078.
22. Bradford, M. M. (1976) A rapid and sensitive method for the quantitation of microgram quantities of protein utilizing the principle of protein-dye binding, *Anal. Biochem. 72*, 248−254.
23. Laemmli, U. K. (1970) Cleavage of structural proteins during the assembly of the head of bacteriophage T4, *Nature 227*, 680−685.
24. Pollard, J. R., and Bugg, T. D. (1998) Purification, characterisation and reaction mechanism of monofunctional 2-hydroxypentadienoic acid hydratase from *Escherichia coli*, *Eur. J. Biochem. 251*, 98−106.
25. Fridovich, I. (1963) Inhibition of acetoacetic decarboxylase by anions. The Hofmeister lyotropic series, *J. Biol. Chem. 238*, 592−598.
26. Cornish-Bowden, A. (1995) *Analysis of enzyme kinetic data*, Oxford University Press, New York.
27. Llanos, L., Briones, R., Yevenes, A., Gonzalez-Nilo, F. D., Frey, P. A., and Cardemil, E. (2001) Mutation Arg336 to Lys in *Saccharomyces cerevisiae* phosphoenolpyruvate carboxykinase originates an enzyme with increased oxaloacetate decarboxylase activity, *FEBS Lett. 493*, 1−5.
28. Tuinstra, R. L., Wang, C. Z., Mitchell, G. A., and Miziorko, H. M. (2004) Evaluation of 3-hydroxy-3-methylglutaryl-coenzyme A lyase arginine-41 as a catalytic residue: Use of acetyldithio-coenzyme A to monitor product enolization, *Biochemistry 43*, 5287−5295.
29. Blackwell, J. R., and Horgan, R. (1991) A novel strategy for production of a highly expressed recombinant protein in an active form, *FEBS Lett. 295*, 10−12.
30. Schlicke, M., and Brakmann, S. (2005) Expression and purification of histidine-tagged bacteriophage T7 DNA polymerase, *Protein Expression Purif. 39*, 247−253.
31. Schlippe, Y. V. G., and Hedstrom, L. (2005) A twisted base? The role of arginine in enzyme-catalyzed proton abstractions, *Arch. Biochem. Biophys. 433*, 266−278.
32. Jelakovic, S., and Schulz, G. E. (2002) Catalytic mechanism of CMP:2-keto-3-deoxy-manno-octonic acid synthetase as derived from complexes with reaction educt and product, *Biochemistry 41*, 1174−1181.
33. Schmitzberger, F., Smith, A. G., Abell, C., and Blundell, T. L. (2003) Comparative analysis of the *Escherichia coli* ketopantoate hydroxymethyltransferase crystal structure confirms that it is a member of the $(\beta\alpha)_8$ phosphoenolpyruvate/pyruvate superfamily, *J. Bacteriol. 185*, 4163−4171.
34. Ash, D. E., Emig, F. A., Chowdhury, S. A., Satoh, Y., and Schramm, V. L. (1990) Mammalian and avian liver phosphoenolpyruvate carboxykinase. Alternate substrates and inhibition by analogues of oxaloacetate, *J. Biol. Chem. 265*, 7377−7384.
35. Gao, Y., and Woo, K. C. (1996) Site-directed mutagenesis of *Flaveria trinervia* phosphoenolpyruvate carboxylase: Arg450 and Arg767 are essential for catalytic activity and Lys829 affects substrate binding, *FEBS Lett. 392*, 285−288.
36. Herzberg, O., Chen, C. C., Liu, S., Tempczyk, A., Howard, A., Wei, M., Ye, D., and Dunaway-Mariano, D. (2002) Pyruvate site of pyruvate phosphate dikinase: Crystal structure of the enzyme-

phosphonopyruvate complex, and mutant analysis, *Biochemistry 41*, 780−787.

37. Gerlt, J. A., and Babbitt, P. C. (2001) Divergent evolution of enzymatic function: Mechanistically diverse superfamilies and functionally distinct suprafamilies, *Annu. Rev. Biochem. 70*, 209−246.

38. Desantis, G., Liu, J., Clark, D. P., Heine, A., Wilson, I. A., and Wong, C. H. (2003) Structure-based mutagenesis approaches toward expanding the substrate specificity of D-2-deoxyribose-5-phosphate aldolase, *Bioorg. Med. Chem. 11*, 43−52.

39. Griffiths, J. S., Cheriyan, M., Corbell, J. B., Pocivavsek, L., Fierke, C. A., and Toone, E. J. (2004) A bacterial selection for the directed evolution of pyruvate aldolases, *Bioorg. Med. Chem. 12*, 4067−4074.

40. Hao, J., and Berry, A. (2004) A thermostable variant of fructose bisphosphate aldolase constructed by directed evolution also shows increased stability in organic solvents, *Protein Eng., Des. Sel. 17*, 689−697.